REPORT
SOLID EARTH: SEISMOLOGY

Earth and Planetary Physics
8: 436–443, 2024
doi: 10.26464/epp2024012

Rapid report of source parameters of 2023 *M*6.2 Jishishan, Gansu earthquake sequence

ZhiGao Yang, Jie Liu*, YingYing Zhang, Wen Yang, and XueMei Zhang

China Earthquake Networks Center, Beijing 100045, China

Citation: Yang, Z. G., Liu, J., Zhang, Y. Y., Yang, W., and Zhang, X. M. (2024). Rapid report of source parameters of 2023 *M*6.2 Jishishan, Gansu earthquake sequence. *Earth Planet. Phys.*, *8*(2), 436–443. http://doi.org/10.26464/epp2024012

Abstract: The *M*6.2 earthquake in Jishishan, Gansu Province, on December 18, 2023, caused extraordinary earthquake disasters. It was located in the northern part of the north–south seismic zone, which is a key area for earthquake monitoring in China. The newly built dense strong motion stations in this area provide unprecedented conditions for high-precision earthquake relocation, especially the earthquake focal depth. This paper uses the newly built strong motion and traditional broadband seismic networks to relocate the source locations of the *M*3.0 and above aftershocks and to invert their focal mechanisms. The horizontal error of earthquake location is estimated to be 0.5–1 km, and the vertical error is 1–2 km. The focal depth range of aftershocks is 9.6–14.6 km, distributed in a 12-km-long strip with SSE direction. Aftershocks in the south are more concentrated horizontally and vertically, while aftershocks in the north are more scattered. The focal mechanisms of the main shock and aftershocks are relatively consistent, and the *P*-axis orientation is consistent with the regional strain direction. There is a seismic blank area of *M*3.0 and above, about 3–5 km between the main shock and aftershocks. It is suggested that the energy released by the main shock rupture is concentrated in this area. Based on the earthquake location and focal mechanism of the main shock, it is inferred that the Northern Lajishan fault zone is the seismogenic structure of the main shock, and the main shock did not occur on the main fault, but on a secondary fault. The initial rupture depth and centroid depth of the main shock were 12.8 and 14.0 km, respectively. The source rupture depth may not be the main reason for the severe earthquake disaster.

Keywords: Jishishan earthquake; earthquake relocation; focal mechanism; strong motion data

1. Introduction

According to the China Seismic Networks Center (CENC), at 23:59 on December 18, 2023, Beijing time, a strong earthquake of magnitude *M*6.2 and focal depth of 10 km occurred in Jishishan County (102.79°E, 35.70°N), Linxia Prefecture, in the southeastern part of Gansu Province. The location of the Jishishan earthquake is in the northern part of China's north–south seismic belt, which experiences frequent tectonic seismic activity. A few kilometers north of the epicenter is the Northern Lajishan fault with Late Pleistocene activity (Yuan DY et al., 2005); to the south is the Late Pleistocene Daotanghe–Linxia fault. This area is an important component of the northeastern edge of the Tibetan Plateau. It is affected by the long-term collision and compression of the Eurasian and the Indian plates and the westward subduction of the Pacific plate to the Eurasian plate (Tapponnier et al., 2001), forming complex landforms and deep structural deformations, developing many deep and large faults such as the East Kunlun fault zone, the north edge of West Qinling fault zone, and the Haiyuan fault zone. Strong earthquakes occur frequently in this region.

Since 1900, a total of 18 earthquakes of magnitude *M*6.0 and above have occurred within 300 km of the Jishishan epicenter (Figure 1), including two earthquakes of magnitudes 8.0–8.9, three of magnitudes 7.0–7.9, and 13 of magnitudes 6.0–6.9. The *nearest* previous earthquake of magnitude 6 or above was the magnitude 6¾ earthquake on February 7, 1936, southwest of Kangle, Gansu Province, which is about 64 km from the epicenter. The *largest* previous earthquake in this vicinity was the 8½ Haiyuan earthquake in Ningxia on December 16, 1920, about 219 km away.

According to the intensity map released by the China Earthquake Administration of the Ministry of Emergency Management (https://www.cea.gov.cn/cea/xwzx/365134/5748483/index.html), the highest intensity reached by the Jishishan earthquake was VIII, covering an area of 331 km^2. This strong earthquake caused great losses; as of 8:00 on December 22, 148 people were known to have been killed. The destruction and death caused by the Jishishan *M*6.2 earthquake exceeded that of most earthquakes of the same magnitude, which aroused widespread social concern.

This paper will combine the waveform data of the traditional broadband seismic network and the new strong-motion seismic network to relocate the source locations of the main shock and of

First author: Z. G. Yang, yzg@seis.ac.cn
Correspondence to: J. Liu, liujie@seis.ac.cn
Received 26 DEC 2023; Accepted 29 JAN 2024.
First Published online 06 FEB 2024.

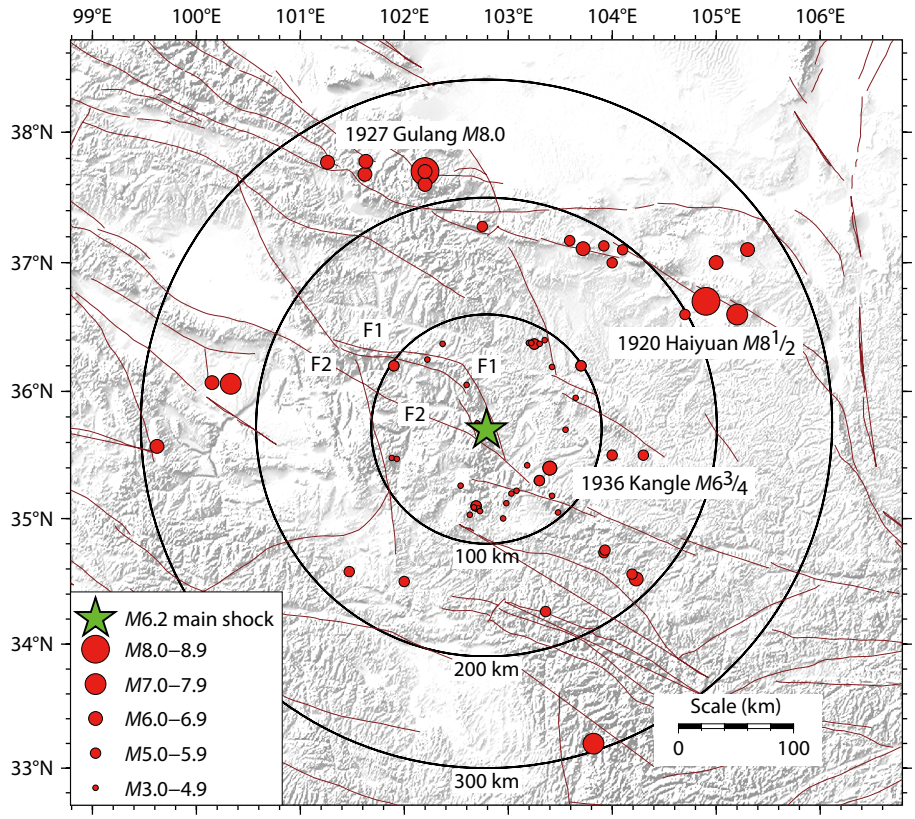

Figure 1. Historical earthquake distribution map of the region surrounding Jishishan. This figure shows locations of historical earthquakes since 1900 as follows: events of strength *M*3.0 and above within 100 km of the main shock; of *M*5.0 or above within 200 km; and of *M*6.0 or above within 300 km. The F1 labeling indicates the Northern Lajishan fault zone; F2 marks the Daotanghe–Linxia fault zone.

aftershocks above *M*3.0 and to invert their focal mechanism solutions. The spatial distribution and focal mechanism characteristics of the Jishishan earthquake sequence that we describe in this paper will provide important data support for subsequent seismic activity assessment and scientific research.

2. Temporal and Spatial Distribution of Earthquake Sequence

As of December 24, 2023, a total of twelve aftershocks of *M*3.0 and above had been recorded, nine of *M*3.0–3.9 and three of *M*4.0–4.9. The largest aftershock had a magnitude of 4.1 (Table 1).

Focal depth is an important parameter in analyzing seismogenic structures. Earthquake location is usually based on velocity-type seismic waveform data, but it is often difficult to find stations near an earthquake's source (especially stations at distances from the epicenter that are less than two times the focal depth). Unless stations happen to be close to an epicenter, the estimated error of focal depth will be relatively large.

A large number of accelerometer stations are included in China's newly built national earthquake intensity rapid reporting and early warning network. Compared with traditional broadband seismic stations equipped with expensive instruments (red triangles in Figure 2), acceleration stations have lower construction and maintenance costs and can be deployed at a higher density. Acceleration stations are equipped with accelerograph or MEMS (Micro-Electro Mechanical System). Blue triangles in Figure 2 indicate strong-motion stations; white triangles indicate MEMS stations. This enhanced network provides unprecedented ability to collect data that improve the accuracy of earthquake source location and depth determination. Different from broadband seismometers that may observe very tiny ground movements, the instrument sensitivity of accelerometer stations is low, detecting only strong ground vibrations in the near field. Their ability to record long-period signals is weak. However, when an epicenter is close, a accelerometer station can obtain high-frequency waveform data with a high signal-to-noise ratio.

Based on the P and S direct wave arrival time data observed at stations within 50 km of the epicenter, this paper uses CRUST1.0 as the velocity model (Laske et al., 2012) and applies SEISAN (Havskov et al., 2020) and HYPOINVERSE (Klein, 2014) software to relocate the source locations of *M*3.0-and-above earthquakes. The errors in picking first arrival of P and S waves are 0.1 s and 0.2 s, respectively, which correspond to propagation distances of 0.6 km (P wave speed 6 km/s) and 0.7 km (S wave speed 3.5 km/s), respectively. After relocation, the horizontal error is estimated to be 0.5–1 km, and the depth error is estimated to be 1–2 km (see Table 1 for relocation results). In order to verify the influence of the layered velocity model, we increased and decreased the overall velocity value of the model by 10%. The obtained horizontal changes in most earthquake source locations were less than 0.3 km, and the changes in earthquake source depth were less than 1 km.

In Figure 3, we plot the relocated earthquakes of *M*3.0 and above

Table 1. Relocated source parameters of the Jishishan earthquake sequence and information on the nearest station that recorded a clear S-wave first arrival.

No.	Earthquake occurrence (Beijing time, GMT+8)	*M*	Latitude (°N)	Longitude (°E)	Depth (km)	Station code	Epicenter distance (km)	$t_{S\text{-}P}$ (s)	Location residual (s)
0	2023/12/18 23:59:30	6.2	35.753	102.826	12.8	N0031	5	1.8	0.15
1	2023/12/19 0:24:49	3.9	37.734	102.783	11.0	N0027	7	1.8	0.14
2	2023/12/19 0:36:18	4.0	35.789	102.759	11.4	N0028	3	1.5	0.10
3	2023/12/19 0:43:12	3.4	35.780	102.770	10.0				
4	2023/12/19 0:56:51	3.4	35.737	102.780	10.5	N0027	8	1.9	0.16
5	2023/12/19 0:59:11	3.1	35.740	102.760	11.4	N0028	9	1.8	0.19
6	2023/12/19 0:59:39	4.1	35.739	102.772	11.5	N0027	8	1.8	0.14
7	2023/12/19 1:10:31	3.2	35.740	102.766	11.2	N0028	9	1.9	0.16
8	2023/12/19 1:20:12	3.2	35.817	102.75	9.6	N0027	1	1.2	0.19
9	2023/12/19 2:10:06	3.2	35.815	102.749	11.0	N0028	1	1.5	0.19
10	2023/12/20 0:32:53	3.4	35.744	102.779	10.6	N0027	8	1.9	0.17
11	2023/12/21 4:02:13	4.1	35.775	102.790	14.6	N0028	6	2.0	0.14
12	2012/12/22 14:43:12	3.0	35.722	102.803	11.9	N0027	5	1.7	0.13

Note: For earthquake 3, above, strong-motion waveform data are incomplete, so relocation could not be carried out; the CENC catalog result is used.

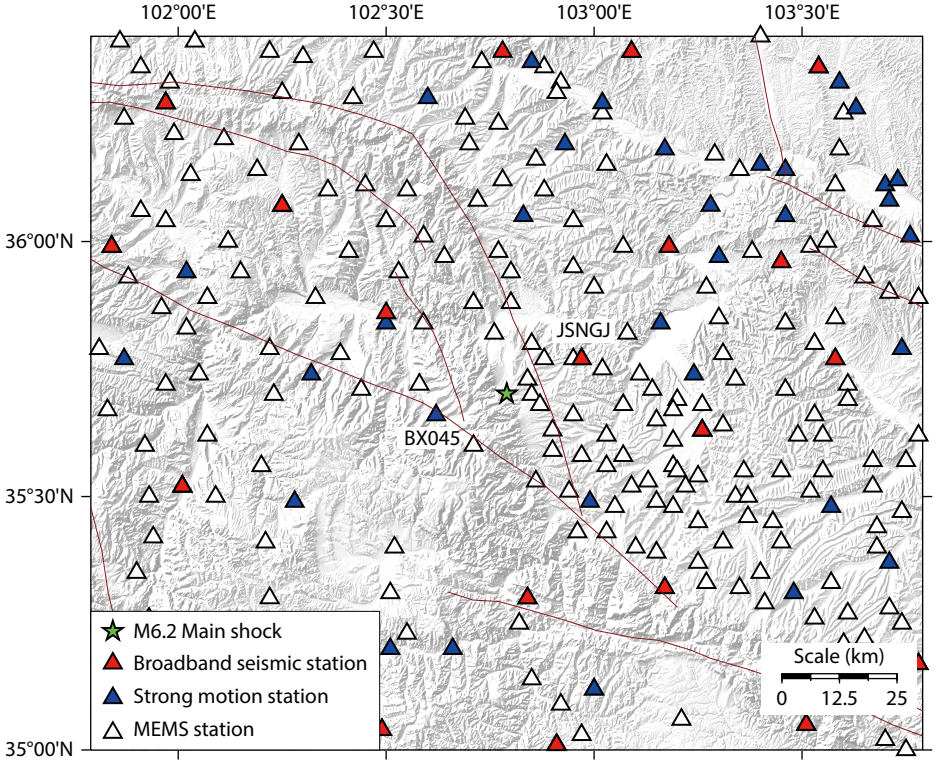

Figure 2. Distribution map of regional seismic and accelerometer stations. Red, blue, and white triangles represent broadband, strong-motion, and MEMS stations, respectively. The nearest broadband seismic station (JSNGJ) and strong-motion station (BX045) codes are marked in the figure. They are about 10 km NE and SW of the main shock (green star), respectively.

with red solid circles; blue solid circles indicate the earthquake catalog produced by the GPSB (Gansu Provincial Seismological Bureau; magnitude scale is M_L). The CENC catalog uses *M* as magnitude scale, which means the magnitude released to the public, and responds only to earthquakes of *M*3.0 and above. The GPSB catalog includes a large number of smaller earthquakes. Figure 3 shows that the spatial distribution of relocated *M*3.0-and-above earthquakes is quite different from that of the GPSB catalog. An important difference is the lack of distribution of *M*3.0-and-above aftershocks near the main shock after relocation. This may indicate that the energy released by the rupture of the main shock was relatively sufficient. After relocation, an area of intensive after-

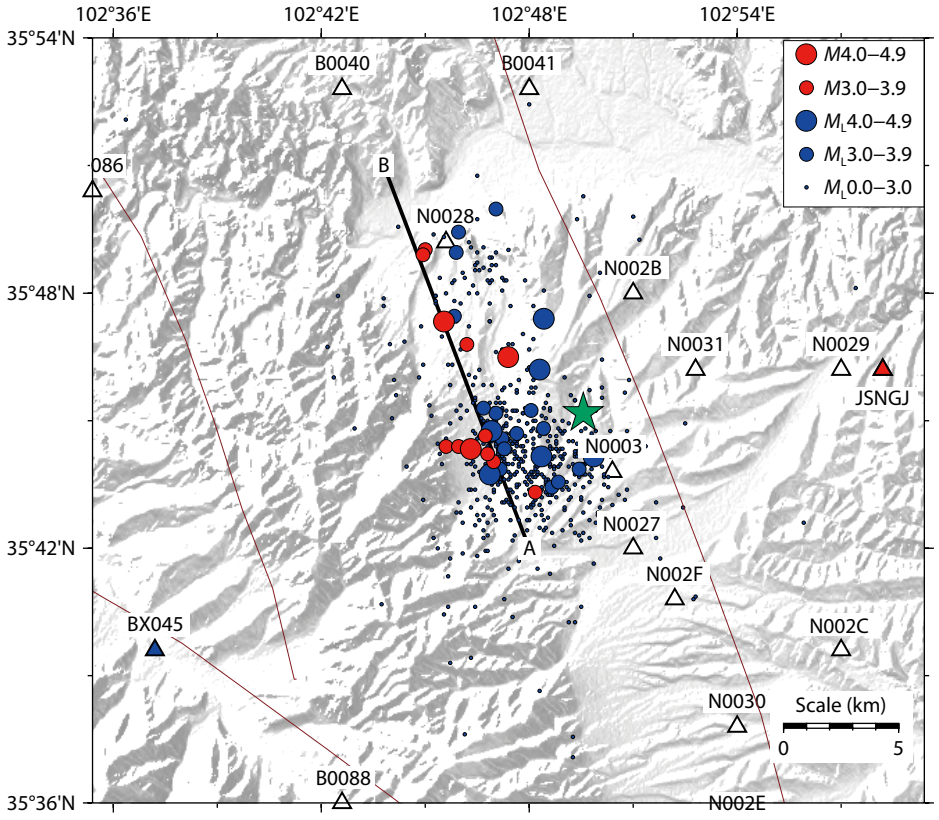

Figure 3. Spatial distribution of earthquake sequence. Relocated earthquakes (magnitudes *M*3.0 and above) are represented by red solid circles; earthquakes of the GPSB catalog are represented by blue solid circles. Triangles represent stations: broadband stations (red), strong motion stations (blue), and MEMS stations (white).

shock activity is seen about 4 km to the west of the main shock, including five *M*3.0–3.9 earthquakes and one *M*4.0 earthquake. Aftershocks in the north are relatively scattered in space, including three *M*3.0–3.9 earthquakes and two *M*4.1 earthquakes (Table 1).

Figure 4 shows the distribution in focal depth of *M*3.0-and-above earthquakes along the fault direction after relocation. It can be seen that there is no obvious difference between the focal depth of the main shock and the nearby aftershocks (Table 1). The focal depths of the aftershock sequence range from 9.6 to 14.6 km, the maximum difference thus being 5 km. The focal depths of the aftershocks near the main shock lie within a very small range, with most clustering around 11 km. The shallowest earthquake, No. 8, and the deepest earthquake, No. 11, are both in the northern aftershock area (Figure 4); their depths are 9.6 km and 14.6 km, respectively.

According to the *M*-*t* diagram of the Jishishan earthquake sequence provided by GPSB (Figure 5), this sequence is of the main shock and aftershock type, with relatively abundant aftershock activity but low magnitude levels. Aftershocks showed fluctuating activity characteristics, but after an *M*4.1 aftershock occurred at 4:00 on the 21st, the aftershock activity attenuated significantly. According to the Gutenberg–Ricker relationship, the *b* value of the earthquake sequence fitted by the maximum likelihood method is about 0.68, and the minimum completeness magnitude is M_L1.4.

Based on the relocated earthquake catalog of *M*3.0 and above,

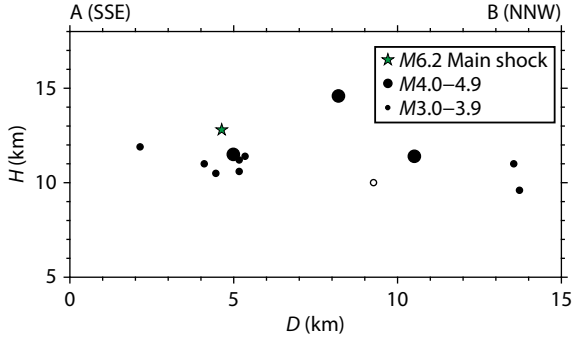

Figure 4. Changes in focal depth along the fault direction of relocated *M*3.0-and-above earthquakes. *D* represents the distance between the projection point of the earthquake on the trend line (the black line in Figure 3 whose endpoints are A and B) and endpoint A. The open circle represents the earthquake No. 3 in Table 1 that has not been relocated.

Figure 6 shows the temporal evolution of aftershock distribution. At the beginning of the earthquake sequence, earthquakes of *M*3.0 and above are distributed throughout the aftershock area (Figure 6). After the 19th, aftershock activity returns to the vicinity of the main shock from north to south, showing that the southern part of the aftershock area is the main area of aftershock activity.

3. Focal Mechanism Solution of Earthquake Sequence

The focal mechanism solution is based on the regional full wave-

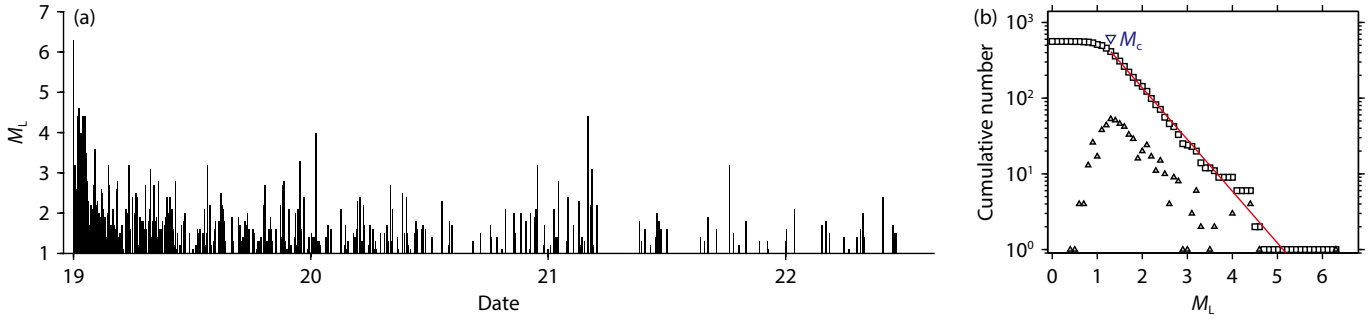

Figure 5. Earthquake sequence *M*-*t* diagram (a) and magnitude–frequency relationship diagram (b). The magnitude scale is the M_L magnitude.

form inversion method (Herrmann et al., 2011; Yang ZG et al., 2023), using broadband waveform data within 300 km of the epicenter to obtain the focal mechanism, moment magnitude and centroid depth of *M*3.0-and-above earthquakes (Table 3, Figure 7). Figure S1 shows the details of the focal mechanism inversion of No. 11 earthquake in Table 3. It includes location map of the broadband seismic stations used during inversion, the theoretical and observed waveform diagrams under the optimal focal mechanism, and the waveform fitting index at different depths.

Table 2 shows the focal mechanism solution, moment magnitude, and centroid depth of the main shock given by other institutions. The main shock focal mechanism of this paper (the strike, dip, and rake angles of the two nodes are 170°/57°/123° and 300°/45°/50°, respectively) is generally consistent with the results published by other institutions. Our result is closer (the Kagan angle is 11.5°; the definition of the Kagan angle can be found in Kagan (1991; 2005)) to the result of GCMT (Global Centroid Moment Tensor); the Kagan angles reported by GFZ (German Research Center for Geosciences) and USGS (United States Geological Survey), are 36.5° and 35.5°, respectively. The moment magnitudes are relatively consistent, with a maximum difference of 0.2. The moment magnitudes given by this article and the USGS are both 5.9, and the moment magnitudes given by GCMT and GFZ are 6.1 and 6.0, respectively. The centroid depth given by USGS is 25.5 km, and that given by this article is 14.0 km. The difference between the two is 11.5 km.

Losses caused by this earthquake were relatively severe, exceeding those from other earthquakes of similar magnitude, partly due to its greater intensity, which reached level VIII.

Focal depth is another important parameter affecting earthquake impact. Focal mechanism inversion, based on regional waveform data, has a relatively short period (10–50 s), and is more sensitive to depth. The centroid depth obtained by the inversion is useful for post-earthquake disaster assessment.

The 2014 M_S6.5 (M_W6.1) earthquake in Ludian, Yunnan, was similar

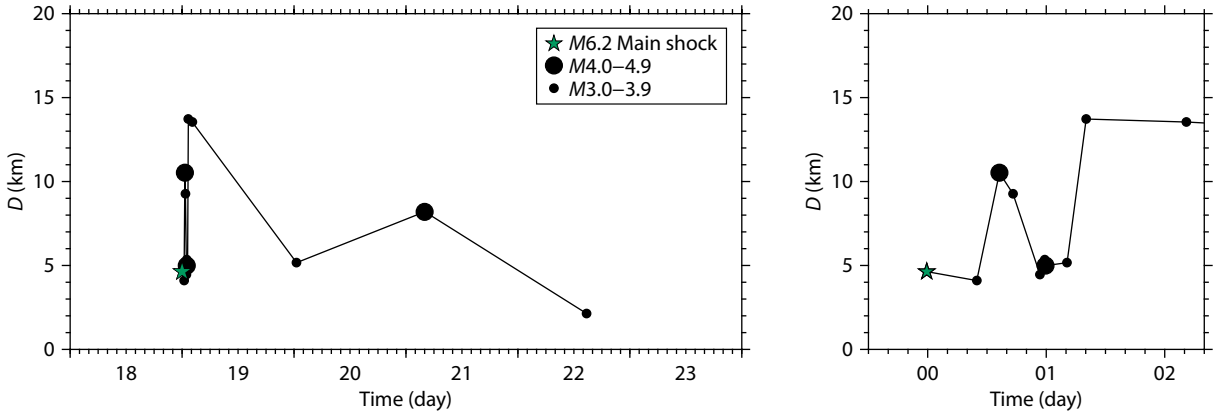

Figure 6. Spatial migration diagram of earthquakes of magnitude *M*3.0 and above along the fault direction. *D* represents the distance between the projection point of the earthquake on the trend line (the black line connecting A and B as two endpoints in Figure 3) and endpoint A. The image on the right shows a partial enlargement of the image on the left at the beginning of the main shock.

Table 2. Focal mechanism, moment magnitude and moment centroid depth given by other institutions.

Institution	M_W	Depth (km)	Strike1/Dip1/Rake1 (°)	Strike2/Dip2/Rake2 (°)	Kagan angle (°)
CENC	5.9	14	170/57/123	300/45/50	
GCMT	6.1	18.9	164/46/122	303/52/62	11.5
GFZ	6.0	19	137/38/79	331/52/98	36.5
USGS	5.9	25.5	333/62/88	156/28/93	35.5

Table 3. Focal mechanism solution of *M*6.2 earthquake sequence.

No.	Date	Beijing time (GMT+8)	Longitude (°N)	Latitude(°E)	Centroid depth (km)	M_W	Stike1/Dip1/Rrake1 (°)	Strike2/Dip2/Rake2 (°)
0	2023/12/18	23:59:30	35.753	102.826	14	5.9	170/57/123	300/45/50
1	2023/12/19	00:24:49	35.734	102.783	9	4.2	125/30/80	125/30/80
2	2023/12/19	00:36:18	35.789	102.759	11	4.2	160/53/106	315/40/70
3	2023/12/19	00:43:12	35.780	102.770	11	3.9	326/66/97	130/25/75
4	2023/12/19	00:56:51	35.737	102.78	11	3.9	290/70/55	174/40/148
5	2023/12/19	00:59:39	35.739	102.772	9	3.9	155/55/95	326/35/83
6	2023/12/19	00:59:11	35.740	102.760	10	3.5	305/55/50	181/51/133
7	2023/12/19	01:10:31	35.740	102.766	11	3.5	250/65/30	146/63/152
8	2023/12/19	01:20:12	35.817	102.750	8	3.5	135/75/70	10/25/142
9	2023/12/19	02:10:06	35.815	102.749	10	3.5	320/50/80	155/41/102
10	2023/12/20	00:32:52	35.744	102.779	10	3.7	270/65/45	157/50/147
11	2023/12/21	04:02:13	35.775	102.790	13	4.1	311/60/93	125/30/85
12	2023/12/22	14:43:13	35.722	102.803	9	3.6	310/70/90	130/20/90

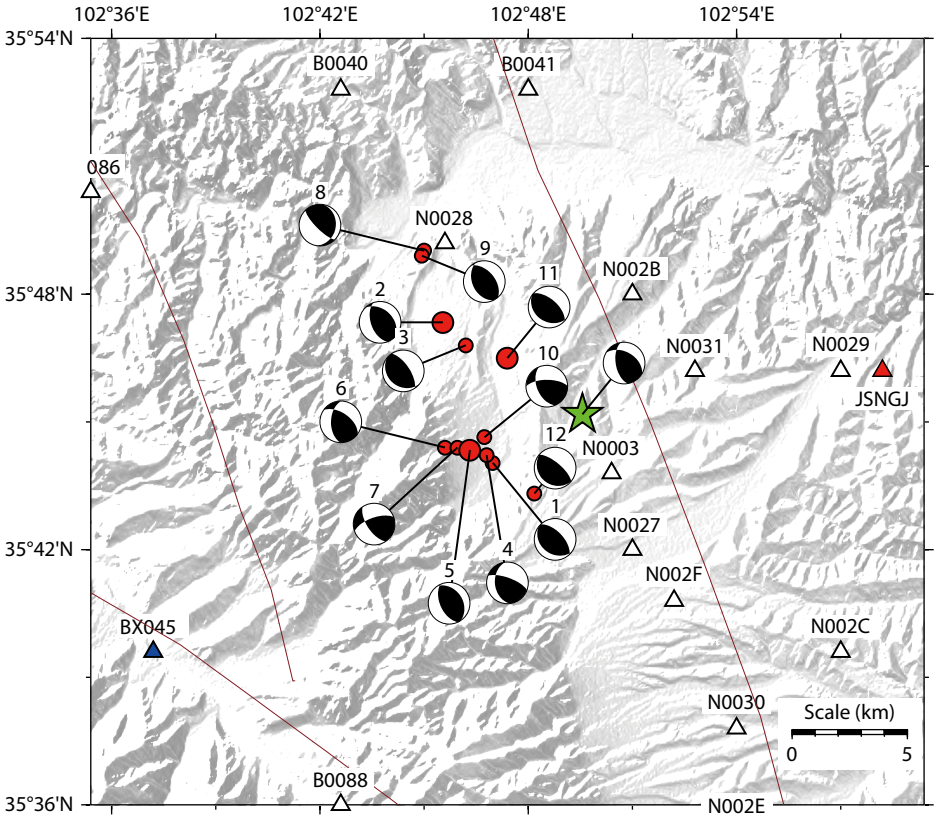

Figure 7. Spatial distribution and focal mechanism of aftershocks of *M*3.0 and above.

in magnitude to this earthquake. That earthquake also caused relatively serious damage. Its ruptures extended from deep to the surface, distributed mainly at depths of 3–10 km (Liu CL et al., 2014). The initial rupture and centroid depths of the Jishishan earthquake, by comparison, were 12.8 and 14.0 km, respectively; taking into account the estimated source depth error, its initial rupture and centroid depths are relatively consistent, which means that the Jishishan earthquake rupture did not spread significantly to shallower depths. Thus the rupture depth of this earthquake may not be the main factor explaining the relatively severe damage it caused.

The main fault line in the Northern Lajishan fault zone (Xu XW et al., 2016, Wu X Y et al. 2023) is only a few kilometers away from the main shock. We have speculated that this fault zone might be the seismogenic structure of this strong earthquake. The dip angle of the main fault in the Northern Lajishan fault zone is 45°–55° (Yuan DY et al., 2005), which is consistent with the focal

plane dip angle of the Jishishan quake's main shock (45° and 57°, respectively). However, according to the regional seismic structure and the direction of aftershock distribution, the focal mechanism node plane 170°/57°/123° is more likely to be the seismogenic fault plane. Based on the depth of the earthquake source and the dip angle of the fault plane, we estimate that the distance between the main shock and the fault line should be more than ten kilometers, not just a few kilometers. Therefore, the main fault is unlikely to be the seismogenic fault. We suggest, instead, that the secondary fault that is about 10 km east of the main fault line may be the seismogenic fault.

The focal mechanism of the aftershock sequence is mainly thrust (Table 3), supplemented by strike-slip, which is generally consistent with the focal mechanism of the main shock. The direction of the principal compressive stress axis of these earthquakes is NEE, consistent with the current direction of crustal movement (Zheng G et al., 2017). The consistency of the earthquake focal mechanism and the direction of regional principal compressive stress are manifestations of the latest activity (late Pleistocene) of the Northern Lajishan fault zone.

4. Summary

Using waveform data from the newly built strong-motion network and broadband seismic network, this paper provides relocation and focal mechanism solutions of 13 *M*3.0-and-above earthquakes in the Jishishan *M*6.2 earthquake sequence in Gansu Province.

The focal mechanism of the main shock is in good agreement with the results of GCMT and others. We infer that the node plane 170°/57°/123° is the real rupture plane; that is, the high-altitude area on the SWW side is the hanging wall, and the relatively low-altitude area on the NEE side is the foot wall. The main shock was very close to the Northern Lajishan fault zone; the focal mechanism type is consistent. We speculate that the Northern Lajishan fault zone is the seismogenic structure of this earthquake. The location of the earthquake source is about several kilometers away from the main fault line of the Northern Lajishan fault zone. According to the dip of the node plane of the focal mechanism, the fault line of the seismogenic structure may be located about 10 km east of the main fault line. The initial rupture and centroid depths of the mainshock are 12.8 and 14.0 km, respectively, which are relatively consistent. We infer that the earthquake rupture did not significantly spread to shallower depths.

The focal mechanisms of the 13 earthquakes in the earthquake sequence show good consistency, exhibiting mainly thrust and a small amount of strike-slip. The main compressive stress direction is NEE, which is consistent with the direction of large-scale surface movement. Aftershocks in the south were more concentrated, while those in the north were more scattered; two of the three aftershocks of *M*4.0 and above occurred in the north. This is the main shock and aftershock type of earthquake sequence, with a *b* value of about 0.68 and a minimum completeness magnitude of about M_L1.4. The depth range of relocated *M*3.0-and-above earthquakes is 9.6–14.6 km. The shallowest and deepest earthquakes were distributed in the northern swarm, which may indicate that the seismic structure in the north is more complex. A blank area of about 3–5 km near the main shock exhibited no aftershocks of *M*3.0 and above; this may be the area where the main shock rupture energy release was concentrated. The energy released by main shock rupture, especially high-frequency energy, is an important factor affecting earthquake disasters. We will use near-field strong motion waveforms to analyze the source spectrum of the main shock and analyse the high-frequency energy release of the main shock in more detail.

Data and Resources

The catalog of earthquakes of *M*3.0 and above, and waveform data of strong earthquake stations and broadband seismic stations, were provided by China Seismic Networks Center (CENC). The catalog of earthquakes with M_L as the magnitude scale was provided by the Gansu Provincial Seismological Bureau and reviewed by CENC. Fault data for this study were provided by Active Fault Survey Data Centre at Institute of Geology, China Earthquake Administration. Most of the figures in this paper were drawn using GMT software (Wessel et al., 2019). Earthquake relocation was conducted by SEISAN and HYPOINVERSE software, based on the CRUST1.0 velocity model. The focal mechanism solution of *M*4.0 earthquakes in the Chinese mainland can be obtained from the seismic data sharing website (https://data.earthquake.cn/datashare/report.shtml?PAGEID=earthquake_dzzyjz), which shares focal mechanism solutions of historical and recent earthquakes of *M*4.0 and above on the Chinese mainland. This study was sponsored by the Spark Program of the Earthquake Science and Technology of China Earthquake Administration (XH23051B). We thank the reviewers for comments and suggestions that improved this manuscript.

References

Havskov, J., Voss, P. H., and Ottemöller, L. (2020). Seismological observatory software: 30 Yr of SEISAN. *Seismol. Res. Lett.*, *91*(3), 1846–1852. https://doi.org/10.1785/0220190313

Herrmann, R. B., Benz, H., and Ammon, C. J. (2011). Monitoring the earthquake source process in North America. *Bull. Seismol. Soc. Am.*, *101*(6), 2609–2625. https://doi.org/10.1785/0120110095

Kagan, Y. Y. (1991). 3-D rotation of double-couple earthquake sources. *Geophys. J. Int.*, *106*(3), 709–716. https://doi.org/10.1111/j.1365-246X.1991.tb06343.x

Kagan, Y. Y. (2005). Double-couple earthquake focal mechanism: random rotation and display. *Geophys. J. Int.*, *163*(3), 1065–1072. https://doi.org/10.1111/j.1365-246X.2005.02781.x

Klein, F. W. (2014). User's guide to HYPOINVERSE-2000, a Fortran program to solve for earthquake locations and magnitude, U.S. Geol. Surv. Open-File Rept. 02-171, revised June 2014.

Laske, G., Masters, G., Ma, Z. T., and Pasyanos, M. (2012). CRUST1.0: an updated global model of Earth's crust. In *EGU General Assembly 2012* (pp. 3743). Vienna, Austria: EGU.

Liu, C. L., Zheng, Y., Xiong, X., Fu, R., Shan, B., and Diao, F. Q. (2014). Rupture process of M_S6.5 Ludian earthquake constrained by regional broadband seismograms. *Chin. J. Geophys. (in Chinese)*, *57*(9), 3028–3037. https://doi.org/10.6038/cjg20140927

Tapponnier, P., Xu, Z. Q., Roger, F., Meyer, B., Arnaud, N., Wittlinger, G., and Yang, J. S. (2001). Oblique stepwise rise and growth of the Tibet Plateau. *Science*, *294*(5547), 1671–1677. https://doi.org/10.1126/science.105978

Wessel, P., Luis, J. F., Uieda, L., Scharroo, R., Wobbe, F., Smith, W. H. F., and Tian, D. (2019). The generic mapping tools version 6. *Geochem. Geophys. Geosyst.*, *20*(11), 5556–5564. https://doi.org/10.1029/2019GC008515

Wu, X., Xu, X., Yu, G., Ren, J., Yang, X., Chen, G., Xu, C., Du, K., Huang, X., Yang, H., Li, K., and Hao, H. (2023). China Active Faults Database and its web system. *Earth Syst. Sci. Data Discuss*. [preprint], https://doi.org/10.5194/essd-2023-119, in review.

Xu, X .W., Han, Z. J.,Yang, X. P., Zhang, S. M., Yu, G. H., Zhou, B. G., Li, F., Ma, B. Q., Chen, G. H., and Ran, Y. K. (2016). Seismotectonic Map in China and Its Adjacent Regions (in Chinese). Beijing: Seismological Press.

Yang, Z. G., Xu, T. R., and Liang, J. H. (2023). Towards fast focal mechanism

inversion of shallow crustal earthquakes in the Chinese mainland. *Earthq. Res. Adv.*, 100273. https://doi.org/10.1016/j.eqrea.2023.100273

Yuan, D. Y., Zhang, P. Z., Lei, Z. S., Liu, B. C., and Liu, X. L. (2005). A preliminary study on the new activity features of the Lajishan Mountain fault zone in Qinghai Province. *Earthq. Res. China (in Chinese)*, *21*(1), 93–102. https://doi.org/10.3969/j.issn.1001-4683.2005.01.010

Zheng, G., Wang, H., Wright, T. J., Lou, Y. D., Zhang, R., Zhang, W. X., Shi, C., Huang, J. F., and Wei, N. (2017). Crustal deformation in the India-Eurasia collision zone from 25 years of GPS measurements. *J. Geophys. Res.: Solid Earth*, *122*(11), 9290–9312. https://doi.org/10.1002/2017JB014465

Supplementary Materials

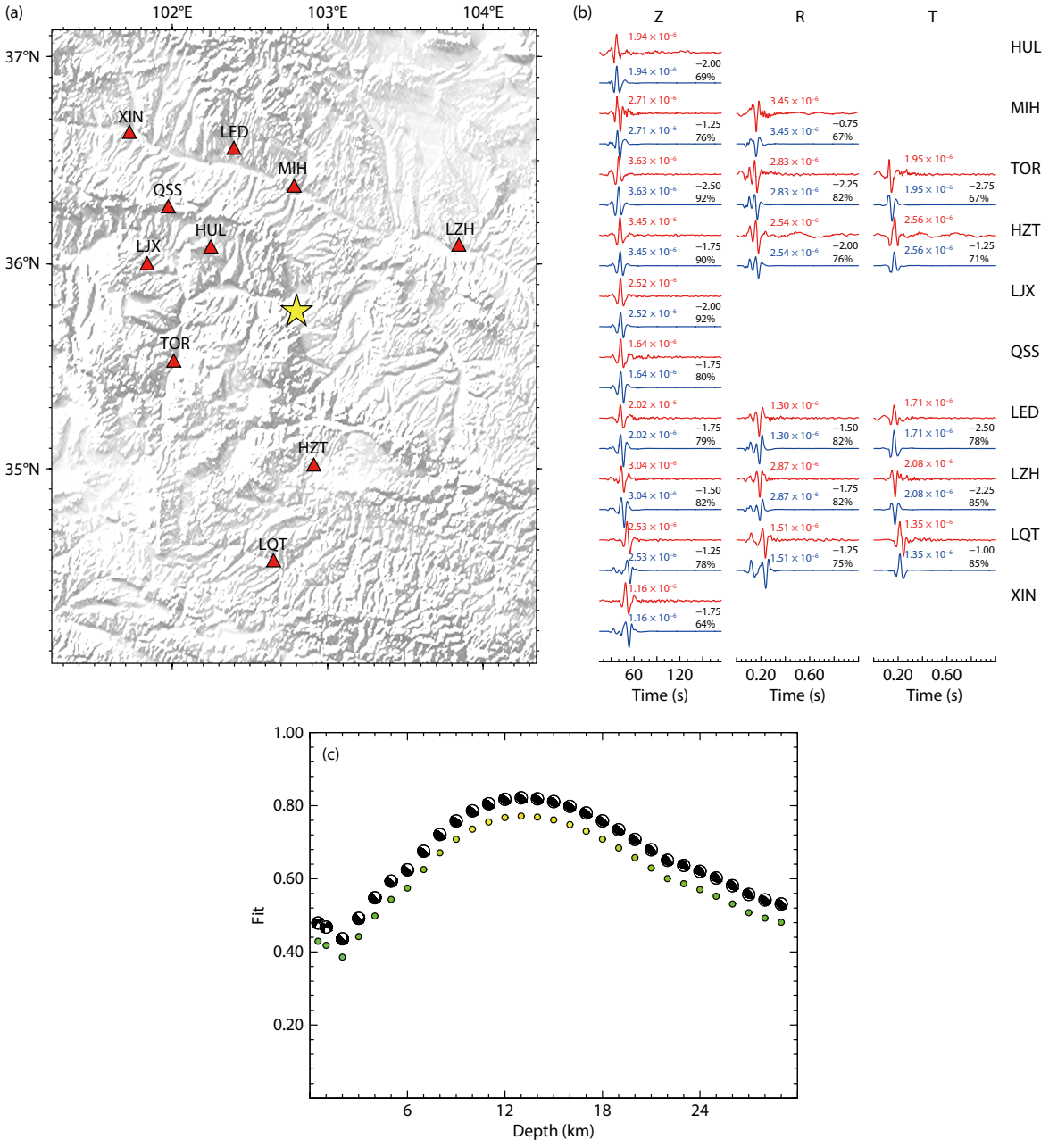

Figure S1. The detail of focal mechanism inversion of the Jishishan *M*4.1 earthquake on December 21, 2023 (No. 11 earthquake in Table 3). (a) shows the locations and codes of the broadband seismic stations used for waveform fitting. (b) presents the observed seismic waveforms (red line) and theoretical seismograms (blue line) of each station after 10–50 s bandpass filtering. The codes of each stations correspond to (a). The numbers on the upper right side of the blue line represent the seismic wave delay time and waveform fitting index from top to bottom, respectively. (c) indicates the fit of observed and theoretical seismic waves as a function of depth.